



# CHORUS

This is the accepted manuscript made available via CHORUS. The article has been published as:

## Structure of drying fronts in three-dimensional porous media

Nima Shokri and Muhammad Sahimi

Phys. Rev. E **85**, 066312 — Published 18 June 2012

DOI: [10.1103/PhysRevE.85.066312](https://doi.org/10.1103/PhysRevE.85.066312)

# The structure of drying fronts in three-dimensional porous media

Nima Shokri<sup>1,†</sup> and Muhammad Sahimi<sup>2</sup>

<sup>1</sup>*Department of Earth Sciences, Boston University, Boston, Massachusetts 02215, U.S.A.*

<sup>2</sup>*Mork Family Department of Chemical Engineering and Materials Science, University of Southern California, Los Angeles, CA 90089-1211 U.S.A.*

Evaporation in a three-dimensional (3D) porous medium, a sand column saturated by water, was studied using synchrotron x-ray tomography. Three-dimensional images of the medium with a resolution of  $7 \mu\text{m}$  were obtained during the evaporation. The entire column was scanned seven times, resulting in nearly  $10^4$  2D cross sections and illustrating the spatial distribution of air, liquid and solid phases at the pore scale. The results were analyzed in order to gain new insights and better understanding of the characteristics of the drying front that was formed when the liquid-filled pores were invaded by air, as well as the structure of the liquid phase as it was dried. The analysis indicates that the liquid phase has a self-similar fractal structure, with its fractal dimension  $D_f$  in all the cross sections being a function of the water content or saturation. In addition,  $D_f$  for the 3D liquid structure, as well as its density correlation function, were computed using the 3D images. A crossover length scale  $\xi$  was identified that separates the fractal regime from the compact geometry. For length scales  $r > \xi$ , the density correlation function approaches asymptotically the water content of the porous medium. The drying front is shown to be rough and multi-affine, rather than self-affine. Its properties were also computed using the 3D images. The roughness characteristics agree with those for imbibition in porous media, but not with those of fracture surfaces and crack lines.

PACS number(s): 47.56.+r, 47.53.+n, 89.75.Fb

<sup>†</sup>e-mail address: nshokri@bu.edu

## I. INTRODUCTION

Understanding the dynamics of drying of porous media, and in particular the structure of the drying front in their pore space, is important to many environmental and engineering phenomena and processes, such as drying of food, wood, paints, biomaterials, building materials, and land-atmosphere interaction that is important to plant growth and microbial activities. The drying process involves invading the pores by air, and replacing the evaporating liquid (e.g. water) by air, which forms the drying front. A large body of literature exists that has focused on various aspects of drying of porous media (see, for example, Refs. [1-12]). The majority of such studies provided evidence that the early stages of evaporation from porous media include a relatively high evaporation rate that is limited by the atmospheric conditions - the so-called stage-1 evaporation - which is supplied by the capillarity-induced liquid flow that hydraulically connects the wet region to the evaporating surface. At a certain characteristic length, which may be estimated by considering the interactions among gravity and the viscous and capillary forces [13], the continuous connection of the liquid phase with the surface breaks, marking the end of stage-1 evaporation. This, in turn, results in lower evaporation fluxes and the onset of stage-2 evaporation, which is dominated by vapor diffusion [14].

Several insightful experiments in two-dimensional (2D) porous media were conducted in the past to advance the fundamental understanding of the mechanisms that govern drying of porous media [2,15-17]. Shaw [15] was among the first who illustrated that a modified form of invasion percolation (IP) [18] with air invading the pores with the weakest capillary forces may be used to describe the drying of a porous medium, and found that the drying front is stable and, locally, has a structure characteristic of the IP. In contrast with the 2D experiments, direct studies of the liquid and air phase distributions in three-dimensional (3D) porous media during evaporation have been very rare, largely due to the difficulties in the visualization. Thus, 3D description of drying of porous media has been limited mainly to numerical simulations. Several groups have developed various pore network models of drying that employ percolation concepts [19,20] to address various aspects of evaporation from 3D porous media at the pore scale [4,21].

Recent advances in imaging techniques have made it possible to take some steps toward direct 3D visualization of drying porous media [6,22,23], illustrating the general pore-scale dynamics of the process. Shokri *et al.* [6], for example, used synchrotron x-ray tomography to

illustrate the key role of the capillarity-induced liquid flow from large pores to the small ones on supplying the liquid to be evaporated. Xu *et al.* [23] used confocal microscopy to study drying dynamics in a 3D granular porous medium, and reported a strong flow from the menisci in the large pores to those in the smaller ones, resulting in abrupt air invasion in parts of the porous medium ranging in size from a single particle to hundreds of particles.

The present paper aims at an improved understanding of drying of porous media by reporting the results of extensive experiments and their analysis. Notwithstanding the progress in describing the evaporation process in 3D porous media, to our knowledge there has been no experimental work that attempted to deduce directly the structure of 3D drying fronts in porous media and the scaling characteristics of the liquid- and air-phase distributions during the process. For example, the fractal dimension  $D_f$  of 3D fronts has been typically estimated by the box-counting method applied to 2D images [24,25], and using the relation between  $D_f$  for 2D cuts from 3D systems. Reporting new results on these aspects is one main objective of this paper.

Thus, in the present paper we present and interpret new experimental data, obtained by direct visualization of water evaporation from a 3D porous medium, using synchrotron x-ray tomography technique. We quantify the structure of the drying front and the scaling characteristics of the liquid structure formed during the drying. We also compare our results with the literature data on imbibition and drainage processes that may be relevant to the drying process. The dynamics of evaporation in porous media similar to what we utilize in the present paper was recently studied by us, with the results reported elsewhere [12].

The rest of this paper is organized as follows. The experimental procedure is described in the next section. The data are then presented in Sec. III, and then analyzed in order to deduce the structure of the water clusters formed during drying. Section IV studies the structure of the drying front, and investigates the possibility that it is rough, with its width having scaling properties. The paper is summarized in the last section.

## II. EXPERIMENTAL PROCEDURE

A cylindrical column, 5 mm in diameter and 12 mm in height, was packed with coarse sand with particle sizes that varied from 0.3 - 0.9 mm. The particle size distribution, determined by a laser diffraction particle-size analyzer, was already given in Ref. [6] and, therefore, will not be

given here. The porous medium's porosity  $\phi$  was 0.38. The column was closed, except at the top where it was exposed to air and evaporation. It was initially saturated by calcium iodide solution (4% mass fraction) to enhance the contrast between air, water and sand. To visualize and study the structural characteristics of the liquid-phase distribution during evaporation, we used synchrotron x-ray tomography. The main advantages of the technique are that, (i) the pore-scale processes can be visualized accurately; (ii) it is a nondestructive method, and (iii) the air invasion patterns can be studied while the liquid flow is in progress, hence enabling us to study the dynamics of the process [12]. The experiments were carried out at the TOMCAT beamline of the Swiss Light Source, Paul Scherrer Institute, Villigen, Switzerland.

The column was scanned with x-rays supplied by the synchrotrons at seven different times after the onset of evaporation. The scanning of the entire column took about 30 min, and yielded 1380 2D gray-scale cross sections of the porous medium. The resolution of the recorded images was  $7 \mu\text{m}$ . The gray-scale images were then segmented in order to delineate the air, water and solid phases. More details about the experiment, synchrotron x-ray measurement, and the segmentation procedure are given by Shokri *et al.* [6,12] and, thus, are not repeated here.

Figure 1 presents typical segmented images that illustrate the air, water and solid phase distributions at a cross section that was 6 mm below the sand surface, at three different times from the beginning of the experiment. We should point out that the wettability of the porous medium and its interaction with fluid content are also important, and affect the evaporation process. They were recently studied in a separate paper [12]. Hence, in this paper we study drying in porous media that are strictly water-wet.

### III. THE STRUCTURE OF THE LIQUID PHASE

As the drying process has some similarities with the IP processes in porous media, the experimental data were analyzed in order to deduce the structural and scaling characteristics of the front and those of the liquid phase as it underwent evaporation.

#### A. Fractal dimension of the liquid phase in two-dimensional cuts

The high-resolution images obtained by synchrotron x-ray tomography indicated that the liquid phase may have a fractal structure as it underwent evaporation. Thus, the images were

utilized for estimating the fractal dimension  $D_f$  of the liquid phase. We first applied the box-counting method [26] to the segmented images of the cross sections in order to calculate the fractal dimension of the liquid phase. As is well-known, in the box-counting method the fractal set is covered by boxes of side length  $r$ . The number  $N$  of such boxes required to cover the pixels occupied with water is then counted and plotted versus  $r$  on a logarithmic scale. If the plot is linear, then  $D_f$  is estimated from the slope of the line, as one has the power law,  $N(r) \propto r^{-D_f}$ .

Examples, taken at two depths below the sand surface, are illustrated in Fig. 2. The box sizes varied from one pixel to the image size. Figure 2 indicates that the fractal dimension of the liquid phase on each 2D cut is related to the position of the cross section or, equivalently, to the water content (saturation  $\times$  porosity), and that  $D_f$  increases as the image plane moves through the bottom of the column where the water content is higher. The same procedure was used to calculate  $D_f$  on all images of the 2D cross sections, measured during each scan of the column.

Variations of the fractal dimension and the water content as a function of depth below the surface are shown in Fig. 3 for seven scans. The fluctuations of the water content profiles in Fig. 3(b) are indicative of the irregular invasion of water-filled pores by air, which includes pinning-depinning of the air-water interface induced by the pore size distribution. Figure 3 shows qualitatively the strong dependence of  $D_f$  on the water content of each 2D cross section, such that higher water contents correspond to larger fractal dimensions, as the liquid phase is more compact at higher water saturations or content.

The computed fractal dimensions of the liquid phase in all the 2D cross sections and their dependence on the water content are shown in Fig. 4. Each scan yielded 1380 cross sections and a total of seven scans were used. Hence, the data shown in Fig. 4 represent the results for 9960 cross sections. Remarkably, all the data are on a single curve described by a power law that expresses the dependence of the fractal dimension  $D_f$  of the liquid phase on the water content  $\theta$ ,

$$D_f \propto \theta^{0.12} . \quad (1)$$

A power law with a small exponent is usually interpreted as being indicative of a logarithmic dependence of  $D_f$  on  $\theta$ . Indeed, as we show shortly,  $D_f$  does increase with the water content or saturation logarithmically.

At the lowest water content, where the water phase is barely connected, the fractal dimension of the phase is close to 1.3. Since the results presented in Fig. 4 are for 2D cuts of a 3D porous medium, one expects to have,

$$D_f(2\text{D cuts}) = D_f(d = 3) - 1 . \quad (2)$$

The results that we obtained for 3D water clusters (see below) are consistent with Eq. (2), if the estimated errors are taken into account. We shall come back to this point shortly. We note that in their experiments in which a liquid metallic alloy (Wood’s metal) invaded a crushed glass sample, Clément *et al.* [26] also reported a saturation-dependent fractal dimension, which also had a low value of close to 1.3, when 2D cuts from the 3D porous medium were analyzed.

Figure 4 also includes the data reported by Chen *et al.* [27] who used magnetic resonance imaging to study the immiscible displacements of oil and water in a porous medium. They carried out drainage experiments - displacement of a wetting fluid by a nonwetting one - and the inverse imbibition experiments, and measured the spatial distribution of the oil phase and the corresponding fractal dimensions in 2D cross sections at various depths below the point at which the the fluids were injected into a cylindrical column. They found that the fractal dimension is not only a function of the water saturation, but also a function of the flow process - drainage or imbibition.

As Fig. 4 indicates, the correlation that we report between the fractal dimension and water content in the drying experiment is in good qualitative agreement with the data on the drainage experiments reported by Chen *et al.* [27]. The similar trends between two seemingly unrelated phenomenon is due to the fact that, in both processes the porous columns that contained a wetting fluid (water) were invaded by a nonwetting fluid - oil in the experiments of Chen *et al.* [27] and air in the present study. Hence, the essence of drying of a porous medium is similar to the invasion of the same porous medium by a nonwetting fluid to displace a wetting one, i.e. the IP process, although some differences between the two phenomena do exist such as, for example, the way the displaced and evaporated fluids leave a porous medium.

## B. Fractal dimension of the liquid phase in three dimensions

Direct experimental estimation of the fractal dimension of 3D liquid (or air) clusters in porous media is rare. Typically, one uses Eq. (2) in order to estimate the fractal dimension

of 3D self-similar fractal structures [24,25,28,29], relying on a series of assumptions that are described by Mandelbrot [28]. Using images obtained by synchrotron x-ray tomography enabled us, however, to estimate  $D_f$  for the 3D water clusters, and to check Eq. (2) for an actual process in porous media that gives rise to fractal structures. Similar to the 2D cuts, the fractal dimension of the 3D water cluster may also be calculated by the box counting method. The only difference with the 2D cuts is that in 3D, instead of using 2D boxes, one must use 3D voxels of various sizes. Then, the number of voxels needed to cover the 3D liquid-phase cluster is counted and plotted versus each voxel size.

Figure 5 presents the estimated fractal dimensions of the 3D water clusters, obtained directly by applying the box-counting method to the clusters. The results do agree with Eq. (2), if the estimated errors are taken into account, particularly for the drier condition at low water contents, although the difference between the two is larger when the porous medium is close to being completely saturated by water.

Note that, as Fig. 5 indicates, the fractal dimension of the liquid cluster in the latter scans, when the medium is drier and the water content is low, is close to 2.5, which agrees with that of 3D IP clusters [18,19]. However, as illustrated by Fig. 5, during the drying the structure of the liquid phase varies with the water content and, thus, its fractal dimension cannot be represented by a single number.

It is straightforward to show that the fractal dimension  $D_f$  is related to the water saturation  $S$  or water content  $\theta$  of a porous medium by [30]

$$D_f = d + a \ln(S\phi) = d + a \ln(\theta) , \quad (3)$$

where  $d$  is the Euclidean dimension of the system,  $\phi$  is the porosity, and  $a = [\ln(r_{\max}/r_{\min})]^{-1/2}$ , with  $r_{\max}$  and  $r_{\min}$  being, respectively, the maximum and minimum pore sizes. As Fig. 5 indicates, Eq. (3) provides excellent fit of the data. If we use Eq. (3) to fit the results for the fractal dimensions of the water clusters in the 2D cross sections, we obtain the results shown in Fig. 4, indicating excellent agreement with the data. As pointed out earlier, such a logarithmic dependence of  $D_f$  of the water content or saturation also explains the small exponent indicated by Eq. (1).

### C. Density correlation function of the liquid phase

It is well known that the density correlation function  $C(r)$  is an accurate tool for characterizing and studying the structure of a fractal cluster [24,26,31]. For a self-similar fractal structure,  $C(r)$  follows a power law

$$C(r) \sim r^{D_f-d} . \quad (4)$$

Physically,  $C(r)$  represents the average water content at a distance  $r$  from a pore occupied by water, according to

$$C(r) = \left\langle \frac{1}{N(r)} \sum_i n_o n_i(r) \right\rangle_o , \quad (5)$$

where  $n_o = 1$  (0) if site  $o$  is occupied (empty),  $n_i(r) = 1$  (0) if site  $i$  at a distance  $r$  is occupied (empty),  $N(r)$  is the total number of available sites located at a distance  $r$  from an occupied site  $o$ , and  $\langle \cdot \rangle$  indicates an average over all the occupied origin sites  $o$  for which all the points at a distance  $r$  remain within the field of view.

For each scan,  $C(r)$  was calculated for 15 equally-spaced cross sections, starting from the surface of the sand column and down to 9.8 mm below the surface (with a spatial increment of 0.7 mm). The calculated  $C(r)$  in each scan was averaged over all the scans. The results are presented in Fig. 6(a), which illustrate two distinct regimes separated around a crossover distance  $\xi$ . For length scales  $r < \xi$ ,  $C(r)$  decreases monotonically and is represented by a power law. The crossover length scale  $\xi$  marks the transition from a fractal structure to a constant density regime in which the water cluster has a compact structure. For length scales  $r > \xi$  the correlation function  $C(r)$  is nearly constant, hence  $D_f = d$ .

When  $r > \xi$ , the density correlation functions in all the seven scans reach an asymptotic value  $C_\infty$  indicated in Fig. 6(a). A constant  $C(r)$  corresponds to a homogeneous liquid-phase distribution and represents the water content of the system. Figure 6(b) presents the asymptotic value  $C_\infty$  of the density correlation function versus the average water content of the porous column, measured by direct 3D visualization of the liquid phase. The results are represented by a straight line at 45°, indicating the equality of  $C_\infty$  and the water content.

#### IV. ROUGHNESS OF THE DRYING FRONT

Similar to many surface and interfaces, ranging from fracture surfaces and crack lines [32,33] to imbibition fronts in porous media [19] that have been shown to be rough and possess scaling properties, the drying fronts in porous media also appear rough. In addition, the similarities

between drying and immiscible displacements in porous media provide additional hints that the drying fronts may be rough. If that is really the case, it is of interest to study its structure, and to understand whether its roughness exponent falls in the range of the values that have been reported for a wide variety of other rough surfaces and interfaces.

The scaling properties of a rough front is typically expressed by a power-law relation between the width  $W(L)$  of the rough surface and the size  $L$  of the window over which  $W(L)$  is computed, where the width is defined by,

$$W(L) = \langle \sum_j [h(r_j) - \langle h \rangle_L]^2 \rangle^{1/2}, \quad (6)$$

where  $h(r_j)$  is the height of the rough surface at point  $r_j$ , and  $\langle h \rangle_L$  its average in a window of size  $L$ . For a rough self-affine surface, one must have

$$W(L) \sim L^\zeta, \quad (7)$$

with  $\zeta$  being the roughness exponent. Equations (6) and (7) have been typically used in the past to study rough surfaces and interfaces, and estimate the roughness exponent  $\zeta$ .

It has, however, been suggested that a more accurate way of studying rough surfaces, as well as gaining additional insights into their structure, is as follows. One first defines a height difference  $\Delta h$  by

$$\Delta h(L) \equiv h(r_j + L) - h(r_j) - \langle h(r_j + L) - h(r_j) \rangle_j, \quad (8)$$

for a window of size  $L$ . Then, according to Bouchbinder *et al.* [34] (see also Refs. [35-37]) one should study the probability density function (PDF)  $P(\Delta h)$  by plotting  $\ln[P(\Delta h)\sigma]$  versus  $\Delta h/\sigma$ , where  $\sigma$  is the standard deviation of the distribution. If a front (in 3D) or a curve (in 2D) is rough and self-affine, then the PDF will be Gaussian and, therefore, its semi-logarithmic plot will be a parabola. If, however, the rough fronts or curves are *multi-affine*, then the tail of the PDF deviates from a parabola. In that case, one constructs a structure function  $S_n(L)$ , defined by

$$S_n(L) \equiv \langle |h(r_j + L) - h(r_j)|^n \rangle_j, \quad (9)$$

which follows the scaling law,

$$S_n(\lambda L) \sim \lambda^{\zeta_n} S_n(L), \quad (10)$$

such that  $\frac{1}{2}\zeta_2 = \zeta$ . For a multi-affine structure,  $\zeta_n \neq \frac{1}{2}n\zeta_2$ , so that for each  $n$  the structure function is characterized by a distinct exponent  $\zeta_n(n)$ .

Using the 3D images that we obtained during the experiments, we constructed the PDF  $P(\Delta h)$  for six box sizes  $L$  (shown in Fig. 7, where  $L$  is in the number of voxels), using all the cross sections in scan 3 (71 min from the beginning of the experiment) in which a front (the interface between the saturated and unsaturated zones) could be discerned clearly. The results are presented in Fig. 7. The parabolas represent the fits of the data. As Fig. 7 indicates, in all the cases the PDF deviates from a Gaussian distribution (parabola in the semi-logarithmic plot), indicating that the drying front is rough and multi-affine, rather than self-affine.

Thus, we computed the structure function  $S_n$  for  $1 \leq n \leq 8$  using the images, based on which the exponent  $\zeta_n(n)$  was estimated. The results, shown in Fig. 8, indicate that for each  $n$  the structure function  $S_n$  is characterized by a distinct  $\zeta_n$ , varying between 0.1 (for  $n = 8$ ) and 0.67 ( $n = 1$ ). There is also a striking similarity between  $\zeta_n(n)$  for the drying front with the corresponding exponents for imbibition fronts in porous media [38] (the authors of Ref. [38] used  $H_n$ , instead of  $\zeta_n$ ). Similar to the results shown in Fig. 8(b), the corresponding exponents for the imbibition front [38] also decreased with  $n$  and were all less than 1.

On the other hand, the results shown in Fig. 8(b) are very different from what has been computed for fracture surfaces [33-37] in that, whereas for the drying fronts  $\zeta_n$  decreases with  $n$ , the corresponding exponents for fracture surfaces *increase* with  $n$  and for  $n \geq 1$  are all greater than 1. This indicates that, contrary to claims often repeated in the literature, not all rough surfaces possess scaling properties that are described by the same value of the roughness exponent, and that the idea of a universal roughness exponent for all rough surfaces cannot be correct.

## V. SUMMARY

Extensive experiments on drying of porous media were carried out, using synchrotron x-ray tomography. The results were analyzed in order to delineate the structure of the clusters formed due to the invasion of water-filled pores by air, as well as the structure and roughness of the drying front. The structure of the water clusters turned out to be fractal. The corresponding fractal dimension  $D_f$  was estimated by using both 2D cuts of the 3D porous medium and by direct analysis of the 3D structure.  $D_f$  was shown to be dependent on the the water content by a simple equation.

We also computed the density correlation function of the liquid phase in several 2D cross

sections along the drying porous medium. The data indicated the existence of a crossover length scale from fractal patterns to compact structures. The drying front was shown to be rough and multi-affine, with its multi-affine properties being very similar to those of imbibition in porous media, but very different from those reported for fracture fronts.

### **ACKNOWLEDGMENT**

N.S. thanks Marco Stampanoni for his support at the Swiss Light Source of the Paul Scherrer Institute (PSI), Villigen, Switzerland. He also gratefully acknowledges funding by the Swiss National Science Foundation Project No. 2000021-113676/1.

- [1] G. W. Scherer, *J. Am. Ceram. Soc.* **73**, 3 (1990).
- [2] I. N. Tsimpanogiannis, Y. C. Yortsos, S. Poulou, N. Kanellopoulos, and A. K. Stubos, *Phys. Rev. E* **59**, 4353 (1999); A. G. Yiotis, I. N. Tsimpanogiannis, and A. K. Stubos, *Dry. Technol.* **28**, 981 (2010).
- [3] P. Coussot, *Euro. Phys. J. B* **15**, 557 (2000).
- [4] A. G. Yiotis, I. N. Tsimpanogiannis, A. K. Stubos, and Y. C. Yortsos, *J. Colloid Interface Sci.* **297**, 738 (2006).
- [5] L. A. Segura, *Drying Technol.* **25**, 1677 (2007).
- [6] N. Shokri, P. Lehmann, and D. Or, *Phys. Rev. E* **81**, 046308 (2010).
- [7] N. Shokri, P. Lehmann, and D. Or, *J. Geophys. Res.* **115**, B06204 (2010).
- [8] E. Shahraeeni and D. Or, *Int. J. Heat Mass Transfer* **54**, 4193 (2011).
- [9] M. Prat, *Chem. Eng. Technol.* **34**, 1029 (2011).
- [10] N. Shahidzadeh-Bonn, A. Azouni, and P. Coussot, *J. Phys. Condens. Matter* **19**, 112101 (2007).
- [11] A. G. Yiotis, D. Salin, E. S. Tajer, and Y. C. Yortsos, *Phys. Rev. E* **85**, 046308 (2012).
- [12] N. Shokri, M. Sahimi, and D. Or, *Geophys. Res. Lett.* **39**, L09401 (2012).
- [13] P. Lehmann, S. Assouline, and D. Or, *Phys. Rev. E* **77**, 056309 (2008).
- [14] N. Shokri and D. Or, *Water Resour. Res.* **47**, W09513, (2011).
- [15] T. M. Shaw, *Phys. Rev. Lett.* **59**, 1671 (1987).
- [16] J. B. Laurindo and M. Prat, *Chem. Eng. Sci.* **53**, 2257 (1996).
- [17] N. Shokri, P. Lehmann, P. Vontobel, and D. Or, *Water Resour. Res.* **44**, W06418 (2008).

- [18] D. Wilkinson and J. F. Willemsen, *J. Phys. A* **16**, 3365 (1983); for recent reviews see, F. Ebrahimi, *Comput. Sci. Eng.* **12** (No. 2), 84 (2010), and Ref. [16].
- [19] M. Sahimi, *Rev. Mod. Phys.* **65**, 1393 (1993); *Flow and Transport in Porous Media and Fractured Rock*, 2nd ed. (Wiley-VCH, Weinheim, 2011).
- [20] D. Stauffer and A. Aharony, *Introduction to Percolation Theory*, 2nd ed. (Taylor & Francis, London, 1994); M. Sahimi, *Applications of Percolation Theory* (Taylor & Francis, London, 1994).
- [21] Y. Le Bray and M. Prat, *Int. J. Heat Mass Transfer* **42**, 4207 (1999); H. Chraïbi, M. Prat, and O. Chapuis, *Phys. Rev. E* **79**, 026313 (2009); T. Metzger and E. Tsotsas, *Chem. Eng. Res. Des.* **86**, 739 (2008); N. Vorhauer, T. Metzger, and E. Tsotsas, *Dry. Technol.* **28**, 991 (2010).
- [22] M. Kohout, Z. Grof, and F. Stepánek, *J. Colloid Interface Sci.* **299**, 342 (2006).
- [23] L. Xu, S. Davies, A. B. Schofield, and D. A. Weitz, *Phys. Rev. Lett.* **101**, 094502 (2008).
- [24] F. Gouyet, M. Rosso, and B. Sapoval, *Phys. Rev. B* **37**, 1832 (1988).
- [25] F. Rezanezhad, W. L. Quinton, J. S. Price, T. R. Elliot, D. Elrick, K. R. Shook, *Hydrol. Process.* **24**, 2983 (2010).
- [26] E. Clément, C. Baudet, E. Guyon, and J. P. Hulin, *J. Phys. D: Appl. Phys.* **20**, 608 (1987).
- [27] J. D. Chen, M. M. Dias, S. Patz, and L. M. Schwartz, *Phys. Rev. Lett.* **61**, 1489 (1988).
- [28] B. B. Mandelbrot, *The Fractal Geometry of Nature* (W. H. Freeman, New York, 1982).
- [29] D. Tang and A. G. Marangoni, *Chem. Phys. Lett.* **433**, 248 (2006).
- [30] B. Yu and J. Li, *Fractals* **12**, 17 (2004).

- [31] J. P. Hulin, E. Clément, C. Baudet, J. F. Gouyet, and M. Rosso, Phys. Rev. Lett. **61**, 333 (1988).
- [32] B. B. Mandelbrot, D. E. Passoja, and A. J. Paullay, Nature **308**, 721 (1984).
- [33] Many papers have reported on studying of roughness of fracture surfaces and crack lines. See, M. J. Alava, P. K. V. V. Nukala, and S. Zapperi, Adv. Phys. **55**, 349 (2006), and M. Ansari-Rad, S. M. Vaez Allaei, and M. Sahimi, Phys. Rev. E **85**, 021121 (2012) for recent summaries.
- [34] E. Bouchbinder, I. Procaccia, S. Santucci, and L. Vanel, Phys. Rev. Lett. **96**, 055509 (2006).
- [35] S. Santucci, K. J. Måløy, A. Delaplace, J. Mathiesen, A. Hansen, J. Ø. H. Bakke, J. Schmittbuhl, L. Vanel, and P. Ray, Phys. Rev. E **75**, 016104 (2007).
- [36] S. Santucci, L. Vanel, and S. Ciliberto, Phys. Rev. Lett. **93**, 095505 (2004).
- [37] P. K. V. V. Nukala, S. Zapperi, M. J. Alava, and S. Simunović, Phys. Rev. E, **76**, 056111 (2007); P. K. V. V. Nukala, S. Zapperi, M. J. Alava, and S. Simunović, *ibid.* **78**, 046105 (2008).
- [38] A. M. Miranda, I. L. Menezes-Sobrinho, and M. S. Couto, Phys. Rev. Lett. **104**, 086101 (2010).

## Captions

FIG. 1. Two-dimensional horizontal cross sections illustrating the distribution of air (white), water (blue) and the solid (black) phases at 6 mm below the sand surface. Numbers at the top indicate the elapsed time from the beginning of the experiment.

FIG. 2. Typical results for estimating the fractal dimension of the liquid phase on two 2D cross sections below the surface. The insets illustrate the cross sections at the corresponding depths below the surface.

FIG. 3. (a) The fractal dimension of the liquid phase, and (b) the water content on each 2D cross section as functions of the depth below the surface. The legend indicates the elapsed time from the beginning of the experiment.

FIG. 4. Dependence of the fractal dimension of the liquid phase in 2D cross sections on the water content of corresponding cross section for the various scans. All the data (a total of 9960 data points) collapse on a single power-law curve with an exponent of 0.12. The data that are not on the curve are from Chen *et al.* [24], representing drainage experiments.

FIG. 5. Estimates of fractal dimensions of the 3D liquid phase in each scan, and their comparison with those obtained from the 2D cross sections.

FIG. 6. (a) The density correlation function  $C(r)$  of the liquid phase in each scan. (b) The asymptotic values  $C_\infty$  of  $C(r)$  versus the average water content in each scan, indicating a 45° line and the equality of  $C_\infty$  and water content.

FIG. 7. The probability distribution function  $P(\Delta h)$  versus  $\Delta h/\sigma$  for six values of the distance  $\ell$  from the inlet of the porous medium and various values of the box size  $L$ . The curves represent the fits of the data to a Gaussian distribution.

FIG. 8. (a) The structure function  $S_n$ , and (b) the dependence of the exponent  $\zeta_n$ , characterizing the power-law behavior of the structure function  $S_n$ , on  $n$ . Symbols correspond to those in FIG. 7.

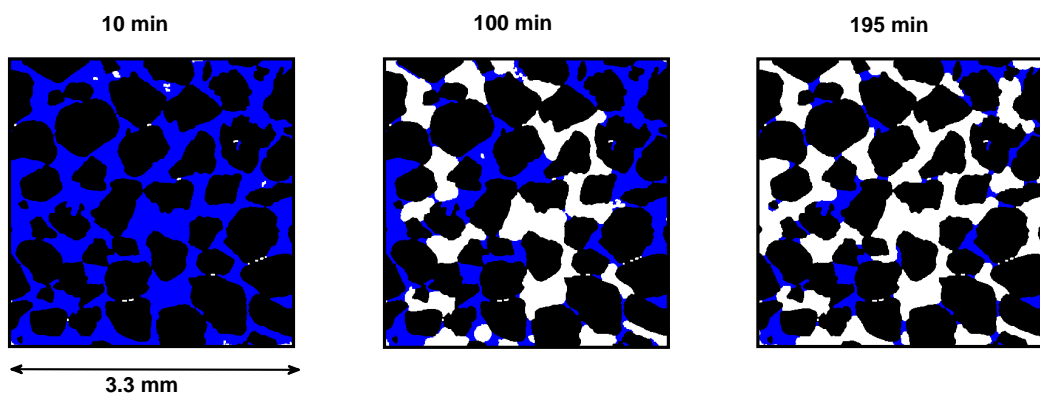


Figure 1

ER10887 04Jun2012

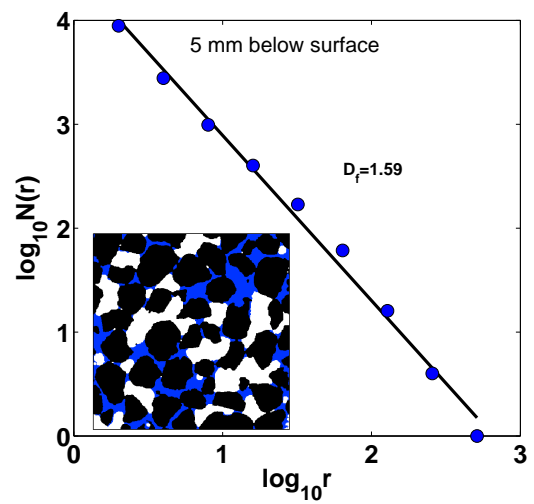
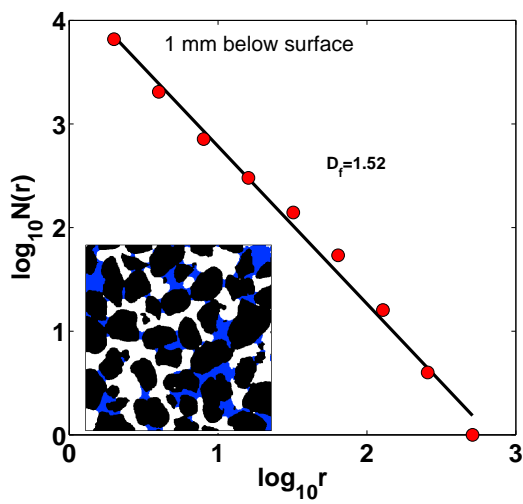


Figure 2

ER10887

04Jun2012

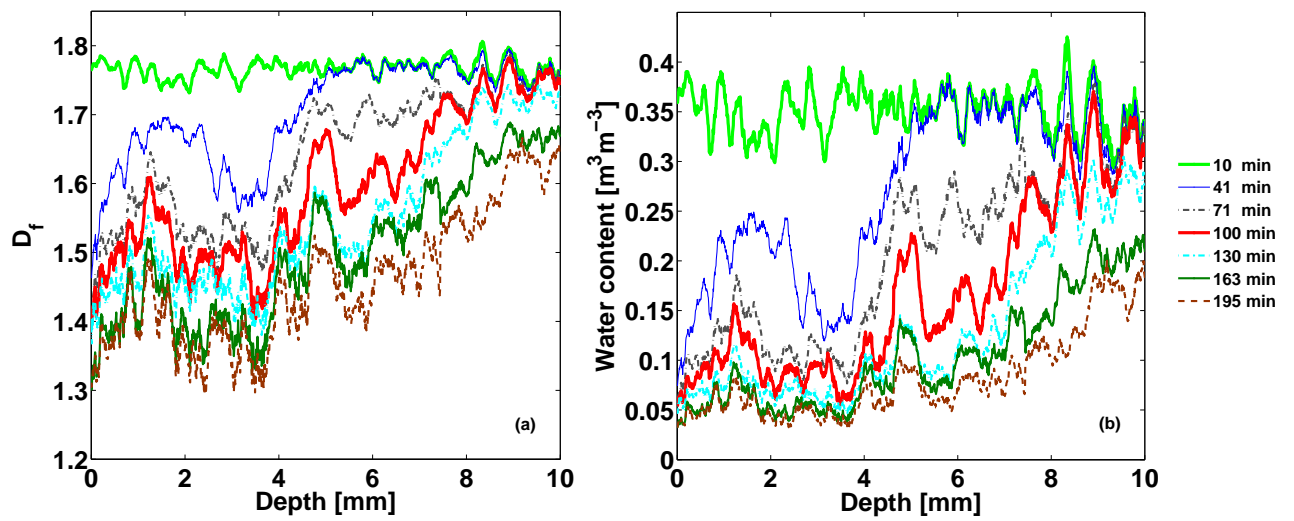


Figure 3

ER10887

04Jun2012

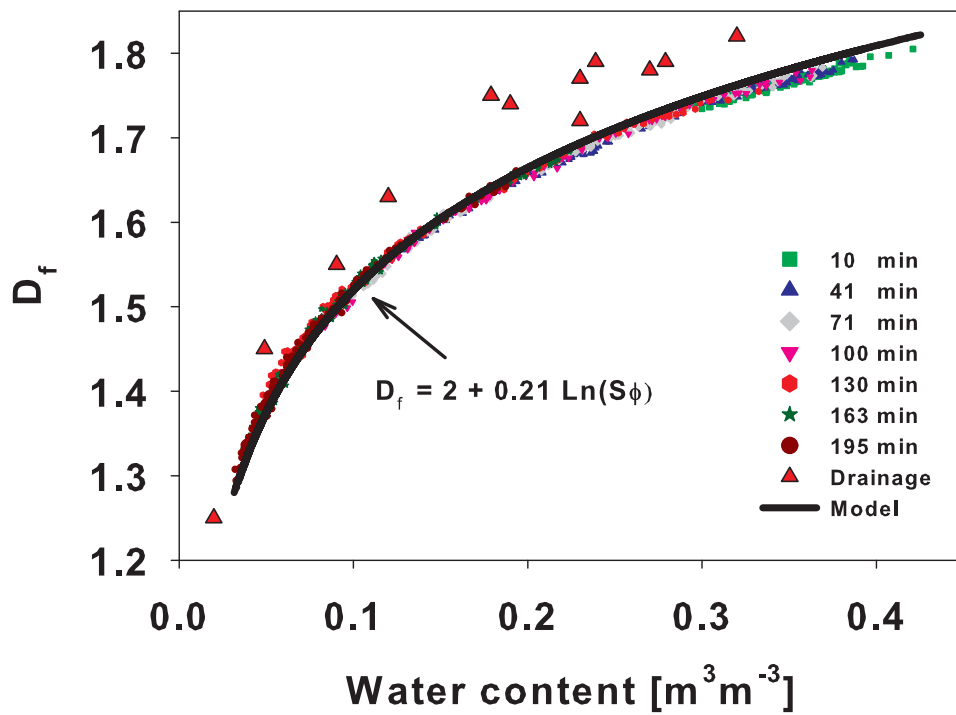


Figure 4

ER10887

04Jun2012

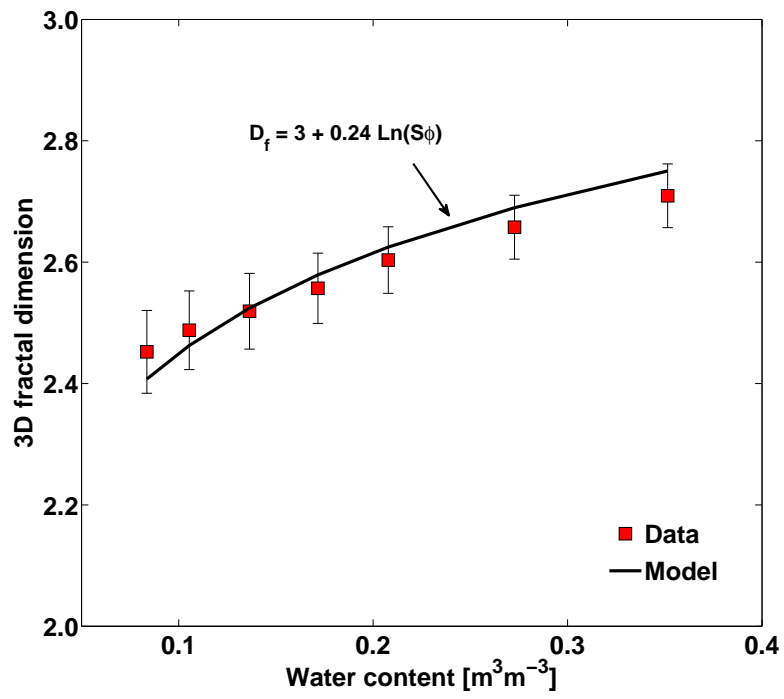


Figure 5 ER10887 04Jun2012

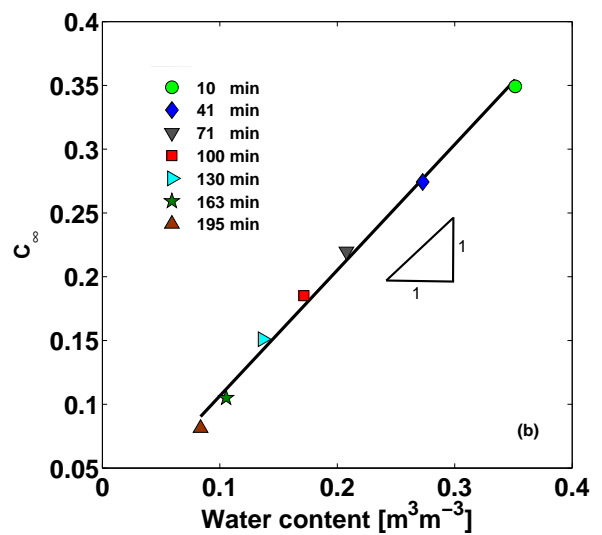
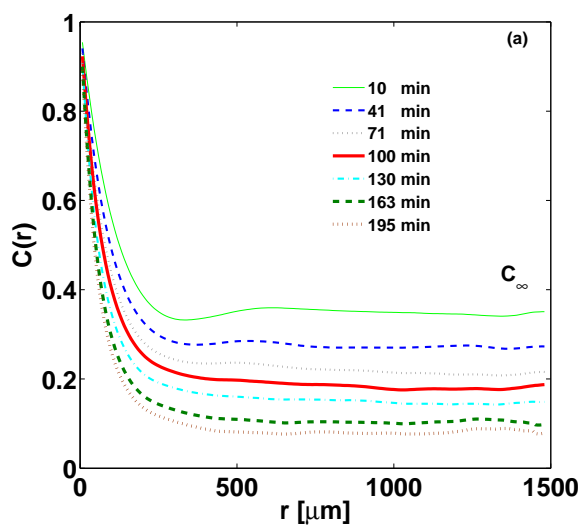


Figure 6 ER10887 04Jun2012

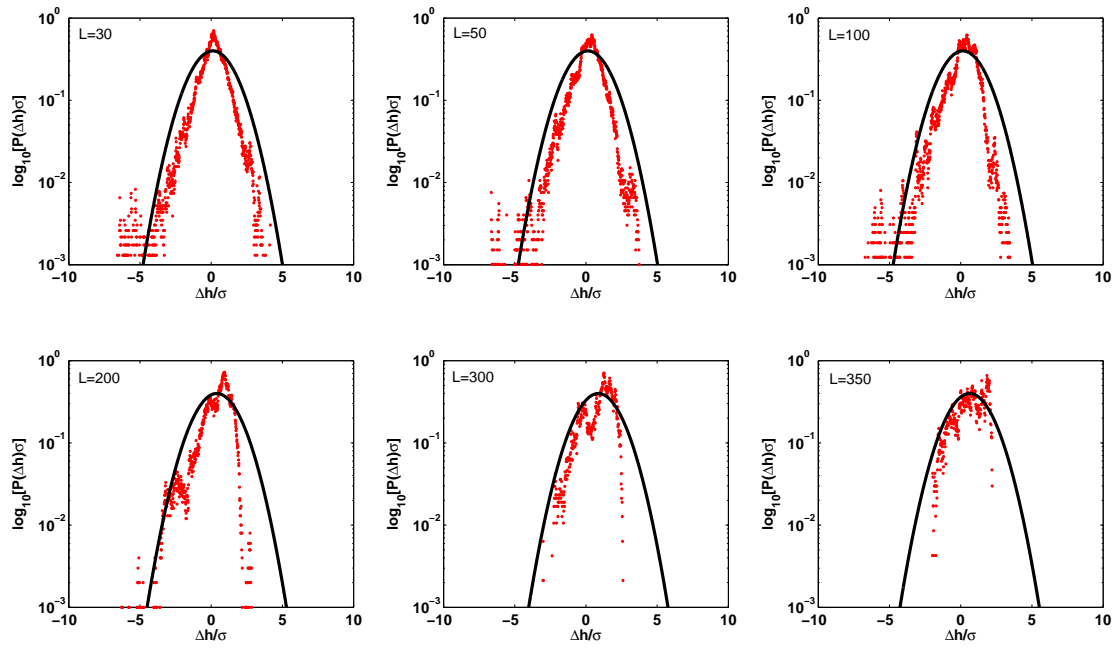


Figure 7

ER10887

04Jun2012

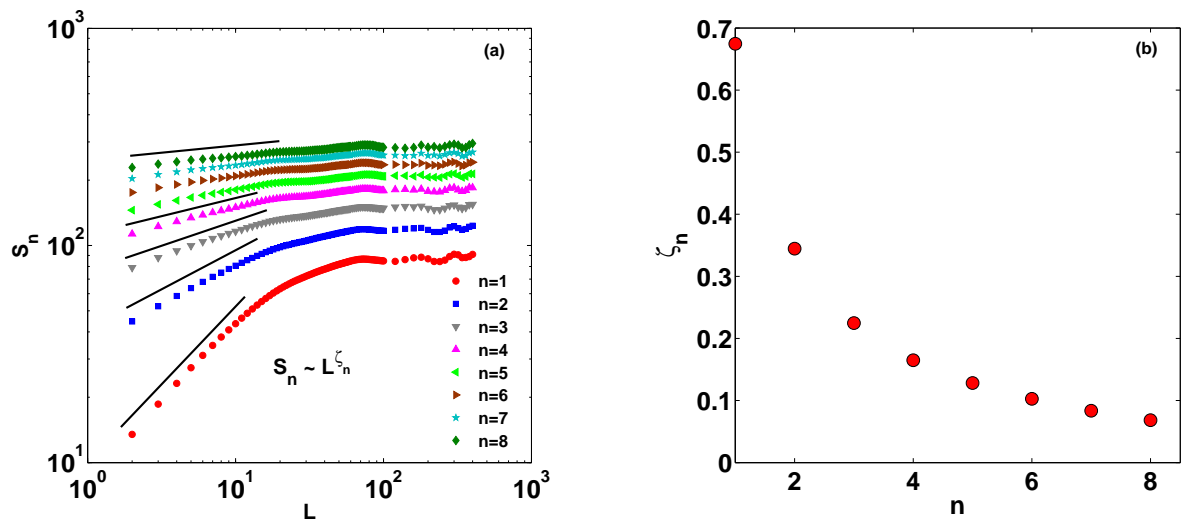


Figure 8 ER10887 04Jun2012